Effect of an Environment-Friendly Depressant on the Flotation of Bastnaesite and Fluorite

Chunlei Guo *, Shaochun Hou , Weiwei Wang , Qiang Li

Posted Date: 5 December 2023

doi: 10.20944/preprints202312.0129.v1

Keywords: Bastnaesite; Fluorite; Sodium alginate; Flotation

Article

Effect of an Environment-Friendly Depressant on the Flotation of Bastnaesite and Fluorite

Chunlei Guo *, Shaochun Hou, Weiwei Wang and Qiang Li

National Key Laboratory of Baiyunobo Rare Earth Resource Researches and Comprehensive Utilization, Baotou 014080, China

Baotou Research Institute of Rare Earths, Baotou, Inner Mongolia 014080, China

* Correspondence: qw884317@126.com

Abstract: To overcome the difficulty of separating bastnaesite from fluorite through the flotation technique, the present study examined the suitability of sodium alginate (SA) as a depressant in the flotation process. The effect of SA on the flotation separation of bastnaesite and fluorite was evaluated using micro-flotation tests, zeta potential measurements, adsorption density measurements, Fourier infrared spectroscopy, and X-ray photoelectron spectroscopy. The micro-flotation results showed that SA exerted a strongly detrimental effect on fluorite flotation, while slightly affecting bastnaesite flotation. The surface chemistry results revealed that the -COO- and HO- functional groups in SA coordinated with Ca^{2+} on the fluorite surface, which induced hydrophilicity and hindered the adsorption in the subsequent collector. However, the interaction of SA with the bastnaesite surface was marginal and did not affect the anchoring of the collector on the surface of bastnaesite. Based on these results, the present study proposes a possible model for the interaction of SA on the surfaces of the two minerals, laying a foundation for the flotation separation of bastnaesite from fluorite with SA as an environmentally benign depressant.

Keywords: bastnaesite; fluorite; sodium alginate; flotation

1. Introduction

The significance of rare earth, a collective term for 17 metal elements (including lanthanides, scandium, and yttrium) has been fully recognized and affirmed owing to its extensive applications as a lubricant for electronics, lasers, superconductors as well as in nuclear industry and other advanced technologies [1–3]. In addition, it is required for enhancing the tactical performance of steel and alloys used in the manufacture of airplanes, tanks, and missiles. Rare earth elements are usually extracted from bastnaesite ($[Ce,La]CO_3F$), which is coeval with fluorite (CaF_2), dolomite, calcite, and other gangue minerals [2–6]. However, their flotation separation is extremely challenging.

The problem of separating bastnaesite from fluorite through flotation is attributed to their similarities as both are micro-soluble salt minerals with similar surface chemical properties. While using hydroxamic acids, such as benzyl hydroxamic acid [7], salicyl hydroxamic acid [8, 9], and naphthalene hydroxamic acid [10], as collectors, fluorite is inevitably entrained into the rare earth concentrates. In the flotation of rare earth ores, researchers have focused mainly on studying and developing collectors. As a result, reports on the depressants for fluorite are scarce. Water glass, as a commonly used inhibitor, provides limited inhibition of fluorite, especially to attain high-grade rare earth concentrates (REO > 58%), which requires that the CaO content should preferably be reduced to less than 5%. Apart from water glass, other depressants including ethylene diamine tetraacetic acid [4], polyepoxysuccinic acid [11], xanthanate gum [5], and sodium lingosulfonate [12] have been reported for the separation of rare earth minerals through floatation. It has been demonstrated that these depressants, containing abundant carboxyl and hydroxyl groups, can form complexes with calcium ions on the fluorite surface, hindering the adsorption of the collector and exerting only a marginal impact on bastnaesite. However, these depressants are expensive and may cause environmental problems; therefore, they have not been validated for application in rare earth

Preprints (www.preprints.org) | NOT PEER-REVIEWED | Posted: 5 December 2023 doi:10.20944/preprints202312.0129.v1

flotation separation, and suitable depressants for flotation separation of bastnaesite from fluorite remain to be further investigated.

Sodium alginate (SA, $(C_6H_7O_6Na)_n$), is mainly found in the cell walls of brown algae [13]. It is a natural, non-toxic, non-hazardous, and biodegradable linear anionic polysaccharide that is widely used in the fields of food industry water treatment and pharmaceuticals [14, 15]. SA belongs to linear block polyanionic polymers, composed of α-L-guluronic acid (G) and β-D-mannuronic acid (M) monomer units with different ratios and connected in different orders (Fig. 1) [14,15]. The application of SA in flotation has been studied in detail. Gu et al. adopted SA to inhibit talc, which led to a reduction in the dosage of the inhibitor carboxymethyl cellulose (CMC) and an increase in the recovery of copper-nickel sulphide [16]. Using SA as an inhibitor, Pan et al. achieved the flotation separation of chalcopyrite from chlorite and serpentine; lithium pyroxene from feldspar; galena from chalcopyrite; and scheelite and apatite from calcite [16–19]. Fu et al. implemented SA in reverse flotation of hematite to improve the grade of iron ore concentrate [20]. These studies underscore the ability of SA, attributed to its structure comprising numerous HO- and -COO- groups, to form complexes with most of the divalent or multivalent metal ions such as Ca^{2+}, Fe^{2+}, Zn^{2+}, Cu^{2+}, Co^{2+}, and Pb^{2+}, leading to the phenomena of gelling and cross-linking, which result in the formation of water-insoluble alginate. However, studies on SA in the flotation of rare earth minerals are scarce.

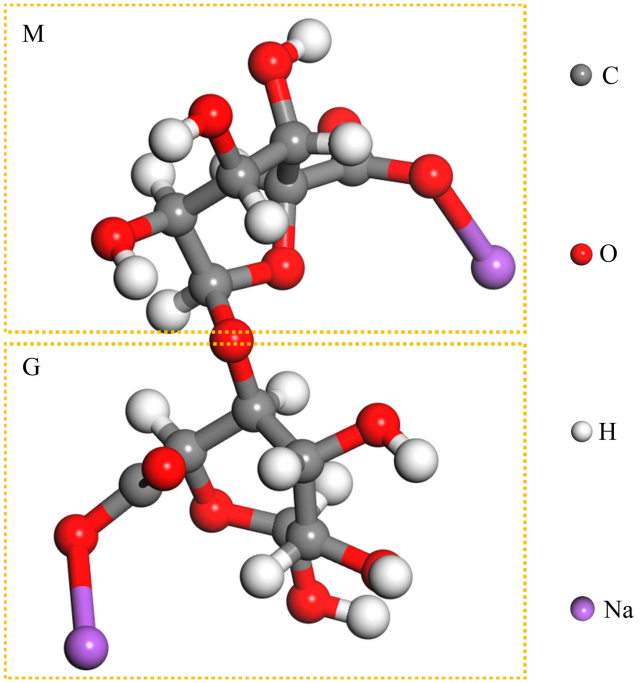

Figure 1. Chemical building blocks of sodium alginate.

In this study, the effect of SA on the flotation separation of bastnaesite from fluorite was investigated to confirm whether SA can be used as a selective depressant for fluorite in flotation separation. The adsorption behaviour of SA on the two minerals was systematically investigated through adsorption density measurements, zeta potential measurements, Fourier infrared spectroscopy (FTIR), and X-ray photoelectron spectroscopy (XPS), based on which a possible adsorption model was proposed.

2. Materials and methods

2.1. Samples and reagents

Highly pure minerals of bastnaesite and fluorite were obtained from Weishan mine in Shandong Province and Bayan Obo mine in Inner Mongolia Autonomous Region, China, respectively. The samples were crushed and sieved, followed by a rigorous shaking using a shaker and a magnetic separator to further improve the purity. Particles sized −75 + 38 μm were used for

Preprints (www.preprints.org) | NOT PEER-REVIEWED | Posted: 5 December 2023 doi:10.20944/preprints202312.0129.v1

micro-flotation and adsorption experiments. In addition, finer particle with a size of −38 μm were further ground to obtain −5 μm sized particles for zeta potential, FTIR, and XPS tests. X-ray diffraction (*X'*Pert PRO, Panalytical, Netherlands) and chemical composition data of the samples are shown in Fig. 2 and Tables 1 and 2. The results indicated that the purity of the bastnaesite and fluorite samples exceeded 95%, while the bastnaesite samples contained a small amount of parisite.

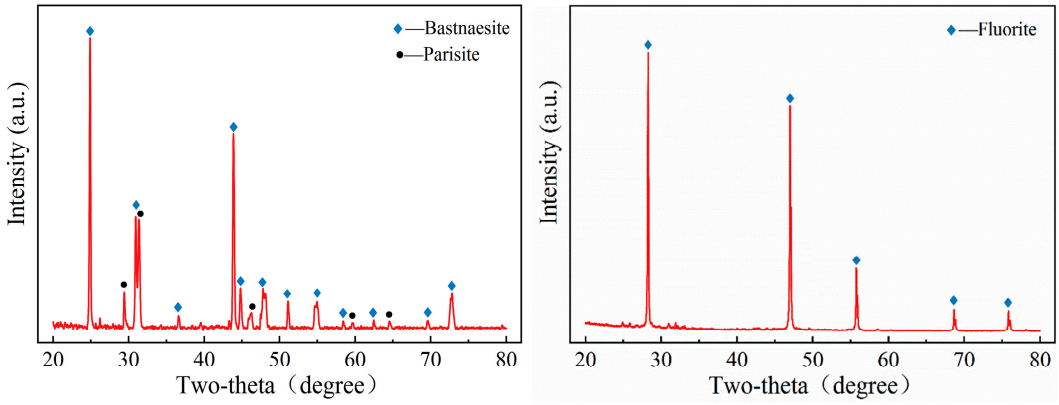

Figure 2. X-ray diffraction pattern of bastnaesite and fluorite samples.

Table 1. Chemical composition of the bastnaesite sample (mass fraction, wt %).

Elements	REO	CaO	F	TFe	Al_2O_3	REE distribution				
						Y_2O_3	La_2O_3	CeO_2	Pr_6O_{11}	Nd_2O_5
Content	70.94	2.30	7.77	0.26	<0.05	0.18	31.40	48.95	4.51	13.13
Elements	Sm_2O_3	Eu_2O_3	Gd_2O_3	Tb_4O_7	Dy_2O_3	Ho_2O_3	Er_2O_3	Tm_2O_3	Yb_2O_3	Lu_2O_3
Content	1.14	0.22	0.42	<0.10	<0.10	<0.10	<0.10	<0.10	<0.10	<0.10

Table 2. Chemical composition of the fluorite sample (mass fraction, wt %).

Elements	F	CaO	BaO	REO	TFe	MgO
Contents	46.45	68.26	0.98	1.51	0.19	<0.10

SA and octylhydroxamic acid (OHA) of analytical grade were purchased from Macklin Biochemical Technology Co., Ltd. (Shanghai, China). Hydrochloric acid (HCl), sodium hydroxide (NaOH), and sodium chloride (NaCl) of analytical grade were procured from Kemiou Chemical Reagent Co., Ltd. (Tianjin, China) for pH adjustment and background electrolyte for zeta potential determination. Deionised water with a resistivity of 18.3 MΩ·cm was used in all experiments and tests.

2.2. Micro-flotation tests

Micro-flotation tests were performed on an XFG-type mechanically agitated flotation machine (Jinlin Exploration Machinery Factory, China). Briefly, 2 g of both minerals was added to a plexiglass tank containing 40 mL of water, and the mixture was agitated for 3 min. Subsequently, the collectors or depressants were added, and the pH value was adjusted using HCl or NaOH solution. The pulp was stirred for 3 min before turning on the air supply, and the froth product was scraped for 4 min. Finally, the concentrates and tailings (residual in the tank) were filtered and dried, respectively, and the minerals were recovered. The concentration of the minerals was determined based on the solid weight of the two products. The average and standard deviation of the recoveries from three parallel sets of tests were calculated and presented.

2.3. Adsorption density measurements

 doi:10.20944/preprints202312.0129.v1

The total organic carbon (TOC) analyser (Multi N/C 2100S, Analytik Jena AG) was employed to measure the adsorption density using the solution depletion method. First, the calibration lines were established, and the correlation coefficients of the fitted equations for total carbon and total inorganic carbon were determined as 0.9999 and 1.0000, respectively. For measurements, the temperature of the cracking furnace and the heating and cooling temperatures were set at 800 °C, 50 °C, and 5 °C, respectively, and the flow rate of oxygen was 180 mL/min. Next, 2 g of the sample was placed in a beaker loaded with 40 mL of water, followed by the agitation for 10 min and the addition of SA solutions of different concentrations. The mixture was stirred for 2h at the desired pH and then filtered through a centrifuge. The TOC contents of the filtrate and the SA stock solution were measured separately. Finally, the average TOC content and relative standard deviation of the three measurements were calculated.

2.4. Zeta potential measurements

The zeta potential of the minerals was measured using Zetasizer Nano ZS90 (Malvern Instrument Co., UK). The suspension was prepared by adding 50 mg of -5 μm minerals to 100 mL of 1.0×10^{-3} mol/L NaCl solution as background electrolyte. After added the desired reagents, the pH of the suspension was adjusted using HCl and NaOH solutions, followed by stirring for 20 min. Finally, approximately 2 mL of the mixture was extracted to measure the zeta potential of the minerals. The results are expressed as the average and standard deviation of values obtained through three independent measurements.

2.5. FTIR

FTIR was conducted using a Bruker-Tensor 27 FTIR spectrophotometer (Bruker Technology Co., Ltd., Germany) in the wave number ranges of 600 and 4000 cm^{-1}. For sample preparation, 1.5 g of the mineral samples was added to a beaker with the desired concentration of SA solution (25.0 mg/L). Subsequently, the pH of the mixture was adjusted to the optimum level for micro-flotation using HCl and NaOH solutions. The mixture was stirred for 1 h, and the suspension was filtered and rinsed three times with deionized water of the same pH. The filter cake was then naturally dried and stored in a desiccator until analysis. For the measurements, KBr discs containing 0.5 wt% of the mineral samples were analysed, with pure KBr discs as a reference.

2.6. XPS

XPS was performed on a Thermo ESCALAB 250XI spectrometer (Thermo Fisher Scientific Co., Ltd., USA) with an Al Kα radiation source. Survey scans of the samples were recorded using an electron analyser with 100 eV passage energy in steps of 1.0 eV and high-resolution scans in a defined binding energy range with a constant passage energy of 20 eV in steps of 0.1 eV. The C1s spectrum at 284.80 eV was applied for the nuclear calibration of all measured spectra. The mineral samples were prepared using the same method used for FTIR measurements.

3. Results and discussion

3.1. Micro-flotation results

The flotation performance of bastnaesite and fluorite was initially investigated as a function of pH and the concentration of OHA as a collector. Fig. 3 depicts the effect of pH on the flotation behaviour of bastnaesite and fluorite, indicating that the recoveries of both bastnaesite and fluorite enhanced with the increasing pH until the pH values were less than 9.0, but decreases sharply in the strongly alkaline pH range. Therefore, the pH value was set to 9.0 in the subsequent experiments, which is consistent with the conclusions reported in the literature [4, 5, 21]. Furthermore, the results indicated that the recovery of bastnaesite was slightly superior to that of fluorite in the set pH range and that OHA is an effective collector for bastnaesite. In addition, the gap of recoveries between bastnaesite and fluorite was not found to be affected by the adjustment of pH value.

Preprints (www.preprints.org) | NOT PEER-REVIEWED | Posted: 5 December 2023 doi:10.20944/preprints202312.0129.v1

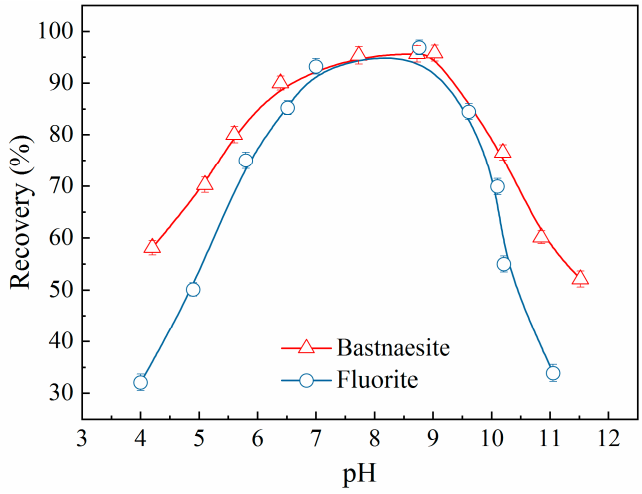

Figure 3. Recovery of bastnaesite and fluorite as a function of pH (*c* (OHA) = 1.57×10^{-3} mol/L).

The effect of OHA concentration on the recoveries of bastnaesite and fluorite is illustrated in Fig. 4. The recovery of bastnaesite and fluorite increased with the increasing concentration of OHA. However, when the OHA concentration exceeded approximately 7.5 × 10^{-4} mol/L, the growth rate tended to decline. Suitable concentrations of OHA (1.57×10^{-4} mol/L) resulted in the recovery rates of over 95% for bastnaesite and fluorite, with the recoveries of both mineral samples being almost indistinguishable at the same OHA concentrations. These results showed the indispensable role of adding a specific depressant in the flotation separation of bastnaesite and fluorite.

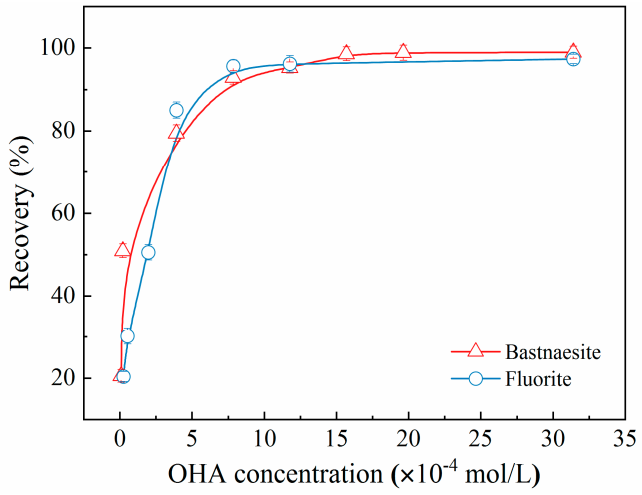

Figure 4. Recovery of bastnaesite and fluorite as a function of OHA concentration (pH = 9.0).

Fig. 5 shows the effect of SA concentration on the flotation performance of bastnaesite and fluorite. With an increase in SA concentration, the recovery of bastnaesite reduced marginally compared to that of fluorite, which dropped dramatically, especially when the SA concentration exceeded 25.0 mg/L. At the SA concentration of 25.0 mg/L, the recovery of fluorite decreased from 95.6% to 15.0%, while that of bastnaesite remained around 80.0%, indicating a disparity in the recovery of two minerals > 65%. These results underscored the suitability of SA for the flotation separation of bastnaesite from fluorite.

Preprints (www.preprints.org) | NOT PEER-REVIEWED | Posted: 5 December 2023 doi:10.20944/preprints202312.0129.v1

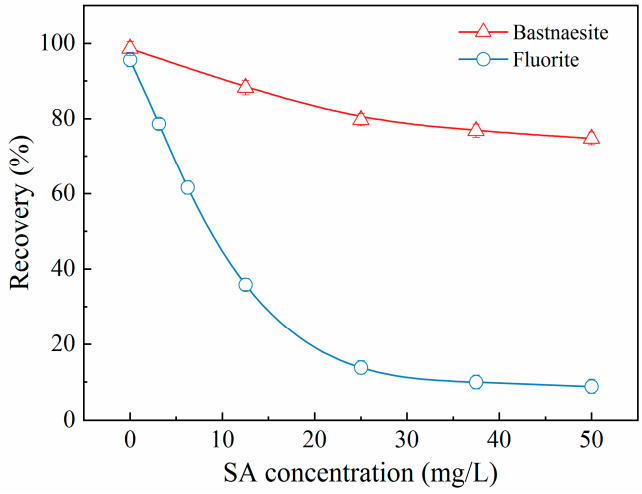

Figure 5. Recovery of bastnaesite and fluorite as a function of SA concentration (c (OHA) = 1.57 × 10^{-3} mol/L; pH = 9.0).

3.2. Adsorption density results

The addition of SA induced its adsorption on the surface of bastnaesite and fluorite (Fig. 6), which in turn caused a significant variation in their recoveries. The adsorption density of SA on the surface of fluorite gradually increased with the increasing SA concentration. However, the increase in adsorption density of SA on the fluorite surface was significant only when the SA concentration exceeded 26.0 mg/L. Moreover, under identical concentration conditions, the adsorption density of SA on the surface of fluorite was higher than that of bastnaesite, which indicated a stronger interaction of SA with fluorite. Considering the abundance of HO- and -COO- groups in SA [16, 19], the higher adsorption density suggested that SA rendered the mineral more hydrophilic and less recoverable.

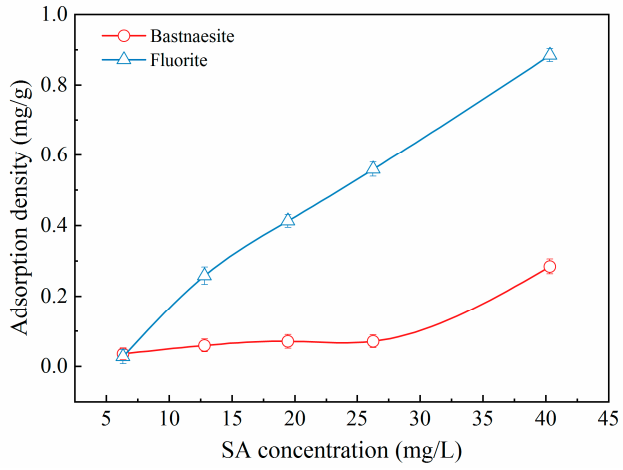

Figure 6. Absorption density of SA on the bastnaesite and fluorite surfaces as a function of concentration.

3.3. Zeta potential analysis

To examine the mechanism of interaction of SA with bastnaesite and fluorite, shifts in the zeta potential of the bilayer on the mineral surface were determined, as shown in Figs. 7 and 8. For the pure fluorite (Fig. 7), the zeta potential decreased progressively with the increasing pH, with isoelectric point (IEP) of approximately 8.4, which aligns with the results of other researchers [5, 22–24]. In conjunction with micro-flotation results, these results indicated that the fluorite surface was negatively charged at an optimum flotation pH value of 9.0.

Preprints (www.preprints.org) | NOT PEER-REVIEWED | Posted: 5 December 2023 doi:10.20944/preprints202312.0129.v1

In the presence of SA (Fig. 7), the zeta potential of fluorite shifted remarkably in the negative direction compared with that of pure fluorite; however, the offset diminished with the increasing pH, indicating that SA adsorption occurred on the fluorite surface. Furthermore, regardless of the presence of chemisorption between the fluorite surface and SA, the electrostatic attraction between the positively charged fluorite surface and the anionic SA component led to a significant shift in the zeta potential of fluorite at pH values below the IEP of fluorite. Conversely, the electrostatic repulsion between the negatively charged fluorite surface and the anionic SA component reversed the effect at pH values above the IEP of fluorite. From another perspective, the deviation of the zeta potential of fluorite at a pH higher than the IEP revealed the existence of SA chemisorption on the fluorite surface.

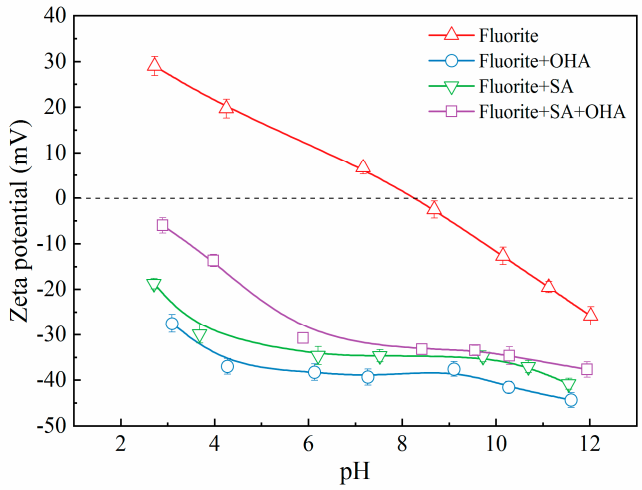

Figure 7. Zeta potential of fluorite with treatment of different reagent schemes as a function of pH (*c* (OHA) = 1.57 × 10^{-3} mol/L; *c* (SA) = 25.0 mg/L).

In the presence of OHA (Fig. 7), the zeta potential of fluorite exhibited the maximal negative shift similar to the trend observed in the presence of SA. In addition, it has been documented that OHA interacts with the fluorite surface through chemisorption and electrostatic adsorption [4].

The minimal zeta potential for fluorite was observed in the presence of both OHA and SA (Fig. 7). The offset of the zeta potential was not significantly altered from scenario in the presence of SA alone, most notably in alkaline conditions. However, the negative shift in zeta potential was smaller than that in the presence of OHA alone. Hence, when SA was preferentially adsorbed on the surface of fluorite to make it negatively charged, then the addition of OHA inhibited its further attachment on the surface of fluorite due to electrostatic repulsion or the spatial steric effect [17]. Consequently, with the adsorption of SA, the surface of fluorite became hydrophilic, and the micro-flotation recovery was diminished.

Preprints (www.preprints.org) | NOT PEER-REVIEWED | Posted: 5 December 2023 doi:10.20944/preprints202312.0129.v1

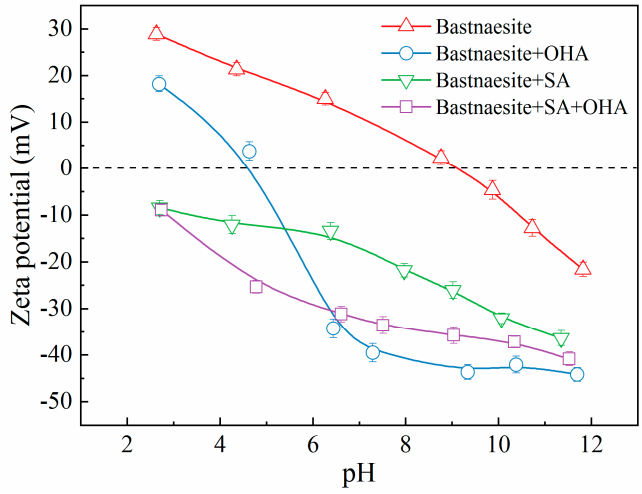

Figure 8. Zeta potential of bastnaesite with treatment of different reagent schemes as a function of pH (c (OHA) = 1.57×10^{-3} mol/L; c (SA) = 25.0 mg/L).

The zeta potential of the pure bastnaesite gradually decreased with the increasing pH (Fig. 8), with the IEP being close to 9.1, which aligns with the results reported in previous studies [4, 25–28]. Combined with the micro-flotation results, these results indicated that the surface of bastnaesite was slightly positively charged at an optimum flotation pH of 9.0.

In the presence of SA (Fig. 8), the zeta potential of bastnaesite deviated considerably from that of pure bastnaesite. However, the shift was mitigated under strongly alkaline conditions. Again, this was indicative of the adsorption of SA on the surface of bastnaesite and the similarity of the interaction between SA and bastnaesite to that of fluorite with SA, as evident from the observed adsorption density.

In the presence of OHA (Fig. 8), the zeta potential of bastnaesite shifted markedly in contrast to pure bastnaesite and bastnaesite with SA, especially at pH higher than 5.0. Nevertheless, the shift was similarly reduced under alkaline conditions. This result implied that the interaction of OHA with the bastnaesite surface stemmed from physical and chemical adsorption [29–31].

The shift in zeta potential of bastnaesite in the presence of SA and OHA versus the zeta potential of pure bastnaesite and bastnaesite with SA is depicted in Fig. 8. This implied that the adsorption of SA on the surface of bastnaesite was relatively weak and that OHA could attach further. However, the gap was reduced at the pH of 9 where the recovery of bastnaesite was optimal compared with that in the presence of OHA. Therefore, the recovery of bastnaesite decreased slightly.

3.4. *FTIR*

To elucidate the mechanism of SA adsorption on the surface of bastnaesite and fluorite, the FTIR spectra of minerals in the presence and absence of SA were recorded (Figs. 9, 10 and 11). For SA, as shown in Fig. 9, the broad band at 3341 cm^{-1} corresponded to the stretching vibration of the hydroxyl (C-OH) group, and the absorption peaks at 2851 cm^{-1} and 2921 cm^{-1} corresponded to the symmetric and antisymmetric stretching vibrations of the -CH- group, respectively [13]. The bands at 1592 cm^{-1}, 1561 cm^{-1}, and 1413 cm^{-1} were ascribed to the antisymmetric and symmetric vibrations of the -COO- group; the weak signal at 1317 cm^{-1} was ascribed to the stretching vibration of -COOH group; and the peak at 1025 cm^{-1} was attributed to the stretching vibration of the C-O-C group [19, 32]. These results affirmed that the main functional groups in SA molecules are -COO-, -OH, and C-O-C, which are strongly hydrophilic due to their polar nature.

Preprints (www.preprints.org) | NOT PEER-REVIEWED | Posted: 5 December 2023 doi:10.20944/preprints202312.0129.v1

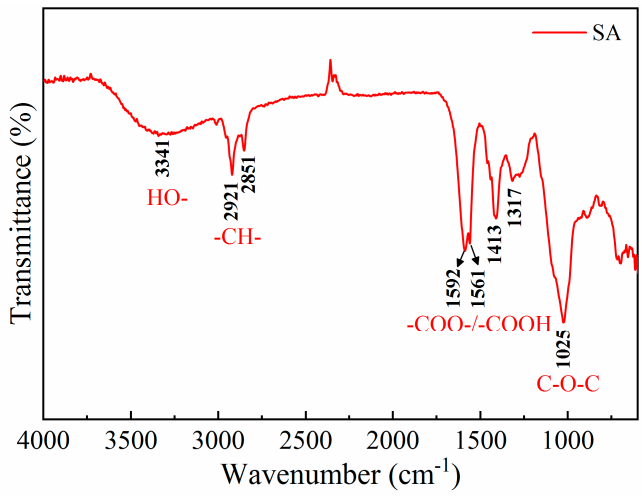

Figure 9. FTIR spectra of SA.

For pure bastnaesite, the bands at 1425 cm^{-1}, 1073 cm^{-1}, 854 cm^{-1}, and 728 cm^{-1} were ascribed to the anti-symmetric stretching, symmetric stretching, out-of-plane bending, and in-plane bending vibrations of the $-CO_3^{2-}$ group, respectively (Fig. 10) [5, 33]. Additionally, no noticeable shift in the characteristic peaks or the new absorption peaks were observed for bastnaesite following SA treatment. These results, along with the adsorption density results, suggested that SA interacted with bastnaesite through physisorption, mainly involving hydrogen bonding or electrostatic interaction [34].

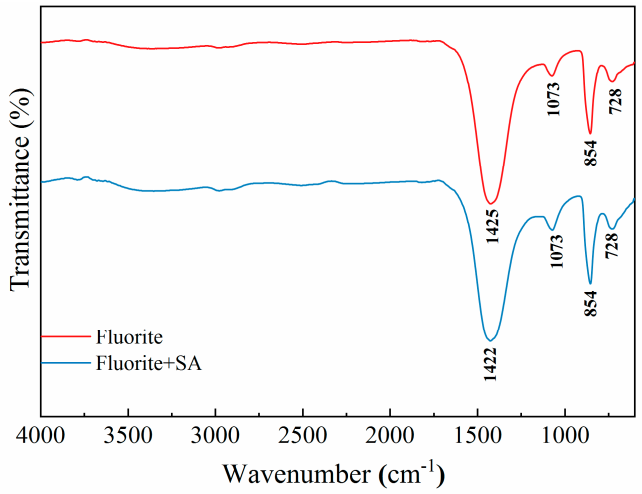

Figure 10. FTIR spectra of bastnaesite in the absence and presence of SA.

For pure fluorite, the characteristic peak was observed at 1033 cm^{-1} (Fig. 11) [35]. With SA treatment, distinct absorption bands were observed for fluorite, which were attributed to the C-OH, -CH-, and -COO- groups in the SA molecule. Furthermore, the characteristic peaks of these groups were shifted to 3411 cm^{-1}, 2980 cm^{-1}, 2904 cm^{-1}, 1604 cm^{-1}, and 1392 cm^{-1}, respectively. In addition, the band of fluorite deviated to 1065 cm^{-1}. Thus, the results indicated that SA interacted with the fluorite surface through chemisorption, which conferred hydrophilicity to the fluorite. Overall, the results of FTIR corroborated the micro-flotation test results.

Preprints (www.preprints.org) | NOT PEER-REVIEWED | Posted: 5 December 2023 doi:10.20944/preprints202312.0129.v1

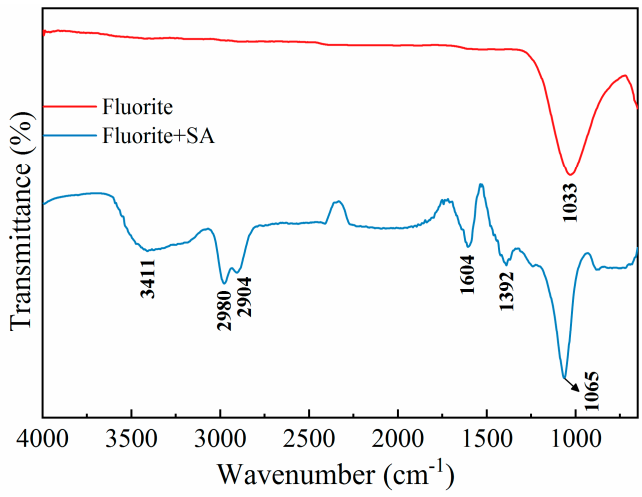

Figure 11. FTIR spectra of fluorite in the absence and presence of SA.

3.5. XPS analysis

To further examine the interaction between SA and minerals, XPS was performed, which helps in understanding the changes in the atomic content and chemical environment of mineral surfaces; the results are presented in Fig. 12 and Table 3. The fluorite surface was relatively rich in calcium (Table 3), which facilitated its easy recovery by fatty acid-based collectors [36, 37]. The low contents of C and O on the fluorite surface inevitably resulted in environmental contamination [5, 21]. With SA treatment, the C and O contents increased by 14.11% and 8.25% to 18.86% and 12.44%, respectively. These results affirmed the occurrence of SA chemisorption on the surface of fluorite. In striking contrast, C and O exhibited higher contents on the surface of bastnaesite. The cationic Ce content was only 4.62%, and in that case was the source of inferior floatability compared to fluorite. With SA treatment, the contents of individual elements did not exhibit significant variations, reflecting the relatively weak adsorption of SA on the surface of bastnaesite. The results were consistent with those of the FTIR analysis.

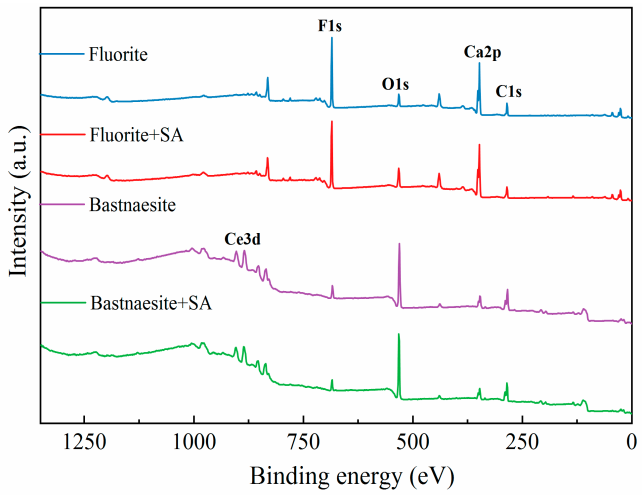

Figure 12. The survey scan XPS spectra of bastnaesite and fluorite in the absence and presence of SA.

Table 3. Atomic content of the surfaces of bastnaesite and fluorite before and after SA treatment.

Mineral	Atomic content (at, %)				
	C1s	O1s	F1s	Ca2p	Ce3d
Fluorite	4.75%	4.19%	37.70%	53.36%	

Preprints (www.preprints.org) | NOT PEER-REVIEWED | Posted: 5 December 2023 doi:10.20944/preprints202312.0129.v1

Fluorite + SA	18.86%	12.44%	27.54%	41.16%	
Bastnaesite	47.16%	41.78%	6.43%		4.62%
Bastnaesite + SA	45.22%	44.76%	5.34%		4.67%

The high-resolution XPS spectra of C1s, O1s, Ce3d and F1s of bastnaesite in the absence and presence of SA treatment are depicted in Fig. 13. In the absence of SA, the C1s spectrum (Fig. 13(a)) consisted of four portions of peaks at 284.80 eV, 286.60 eV, 287.95 eV, and 289.57 eV attributed to the C-C, C-O-C, C-O=C, and bastnaesite components, respectively [4,5,21]. The peaks at 531.50 eV and 533.42 eV (Fig. 13(b)) were assigned to the C-O and C=O components, respectively [38, 39]. The Ce3d region (Fig. 13(c)) of bastnaesite had spin-orbit components that were well separated into $Ce3d_{5/2}$ and $Ce3d_{3/2}$ units, and the peaks at 885.78 eV and 904.39 eV were the primary line of bastnaesite [22, 40, 41]. Since Ce atoms held only one 4f electron, the inner electrons of $Ce3d_{5/2}$ and $Ce3d_{3/2}$ were ionized when forming bastnaesite with F, C, and O atoms, which induced the splitting of the characteristic peaks of Ce, leading to the matching peaks of $Ce3d_{5/2}$ and $Ce3d_{3/2}$ at 882.30 eV and 900.35 eV, respectively. In addition, the F1s peak (Fig. 13(d)) was located at 684.45 eV [38]. In the presence of SA, the binding energies of C1s, O1s, Ce3d, and F1s of bastnaesite all exhibited a very slight shift, which indicated that SA did not bind to the surface of bastnaesite.

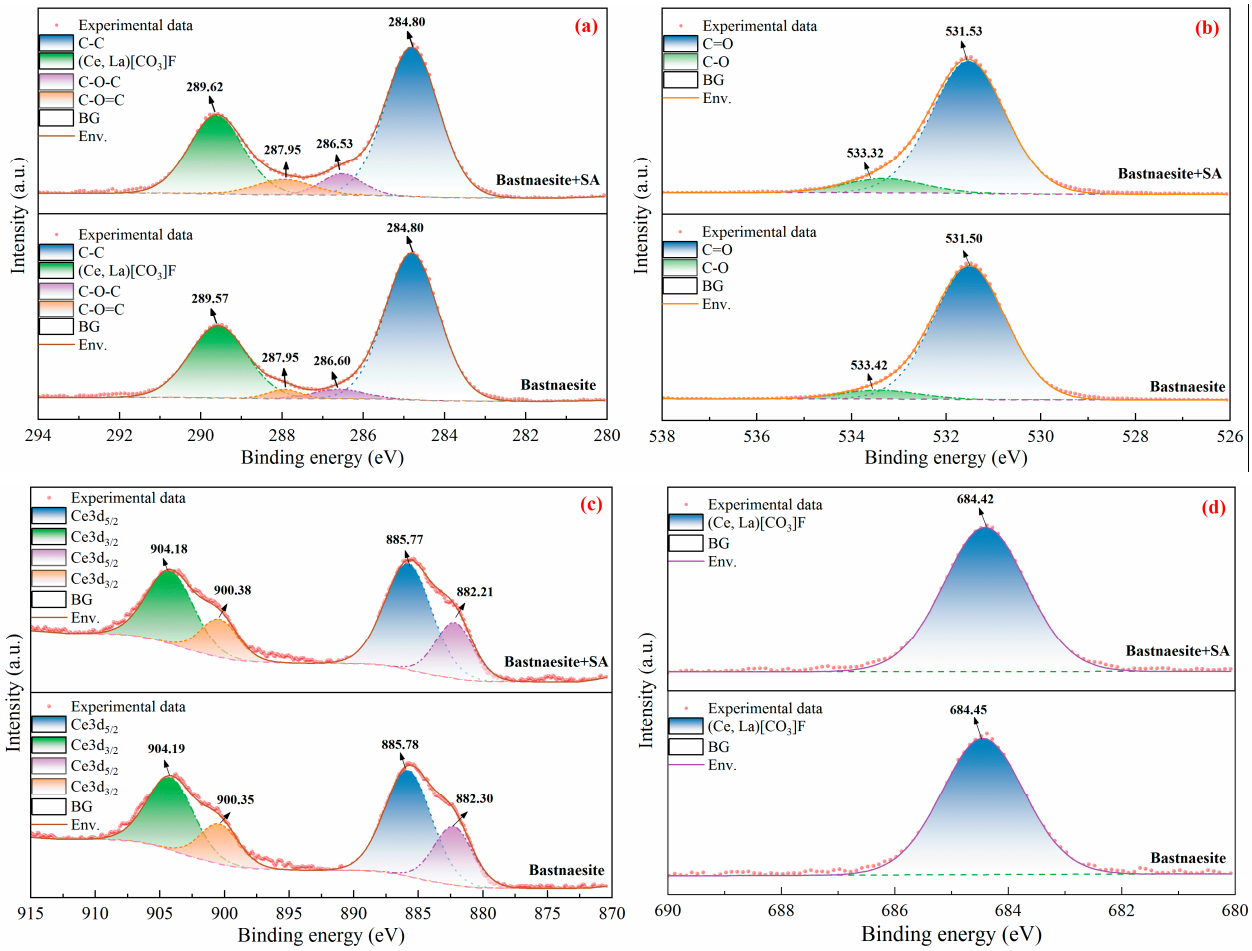

Figure 13. The high-resolution XPS spectra of (a) C1s, (b) O1s, (c) Ce3d, (d) F1s of bastnaesite in the absence and presence of SA.

The high-resolution XPS spectra of C1s, O1s, Ca2p and F1s of fluorite in the absence and presence of SA are shown in Fig. 14. In the absence of SA, the C1s peaks (Fig. 14(a)), accounting for inescapable contamination, were located at 284.80 eV, 286.47 eV, and 289.08 eV, which were attributed to the C-C, C-O-C, and C-O=C components, respectively [4, 21, 38]. In the presence of SA, the C1s binding energies in the C-O-C component underwent a significant shift, reducing to 288.65

Preprints (www.preprints.org) | NOT PEER-REVIEWED | Posted: 5 December 2023 doi:10.20944/preprints202312.0129.v1

eV. The altered binding energy signified a change in the chemical environment of C atoms in the C-O-C composition. In the absence of SA, the O1s peaks (Fig. 14(b)) comprised C=O, C-O, and Ca-O components at 531.54 eV, 533.04 eV, and 530.35 eV, respectively [21]. In the presence of SA, these peaks were maintained at 531.91 eV, 533.39 eV and 530.94 eV. The pronounced chemical shift of the O1s component indicated that the O atoms in the SA molecular structure bonded to the surface of fluorite, signifying the adsorption of SA on fluorite surface. In the absence of SA, the peaks of Ca2p (Fig. 14(c)) split into two spin-orbit splitting peaks, namely $Ca2p_{3/2}$ and $Ca2p_{1/2}$, at 348.56 eV and 352.10 eV, respectively [42–44]. In the presence of SA, the binding energies of the two peaks were off-shifted to 348.12 eV and 351.66 eV, respectively. Combined with the changes in binding energies of the O1s peaks, these results indicated that the O atoms in the SA molecular structure were chemically bound to the Ca atoms on the fluorite surface. In contrast, the binding energies of the F1s peaks (Fig. 14(d)) remained markedly unchanged in the absence and presence of SA, which indicated that SA did not interact with F atoms on the fluorite surface.

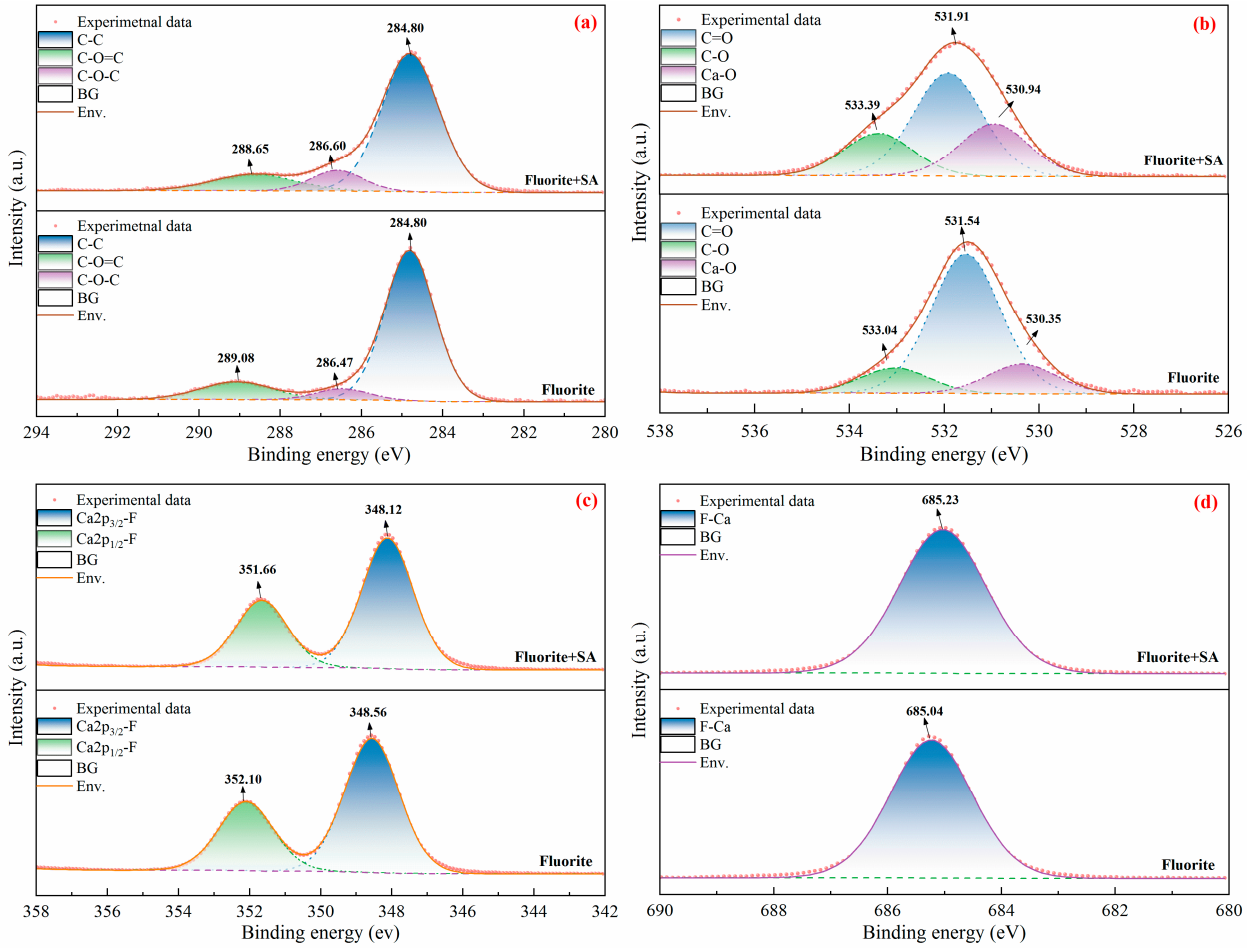

Figure 13. The high-resolution XPS spectra of (a) C1s, (b) O1s, (c) Ca2p, (d) F1s of fluorite in the absence and presence of SA.

3.7. Discussion

The results of flotation experiments and surface analysis clearly indicate SA chemically interacts with the fluorite surface but interacts weakly with the bastnaesite surface. These results are consistent with those of Wei Chen et al. who investigated the flotation separation of calcite and fluorite from scheelite; apatite from calcite; and chalcopyrite from galena [18, 32, 17]. A possible model for the interaction of SA with fluorite and bastnaesite is illustrated in Fig. 14. Under alkaline conditions, chemically active functional groups in SA, such as -COO-, and HO-, coordinate with the

Preprints (www.preprints.org) | NOT PEER-REVIEWED | Posted: 5 December 2023 doi:10.20944/preprints202312.0129.v1

mineral surface to form a cross-linked network structure, resulting in the formation of a hydrogel that boosts the hydrophilicity of the mineral surface [45].

In the flotation systems for fluorite or bastnaesite, the crystal structure of the mineral is a key factor that affects the ability of SA to exert selective inhibition. Bastnaesite crystals are arranged hexagonally, with Ce and F atoms in the same plane and alternating CeF^{2+} and CO_3^{2+} layers [46]. The (100) plane is the most stable cleavage plane, where the coordination number of Ce atoms reduces from nine to five. In contrast, fluorite crystals are attributed to a cubic crystal system, with Ca atoms closely packed along the planes and F atoms filling in the tetrahedral interstitial positions [47, 48]. The (111) plane is the most stabilized cleavage plane of fluorite, wherein the coordination number of Ca atoms reduces from eight to four. The ionic radii of Ce^{3+}, Ca^{2+}, F^-, and O^{2-} are 1.03 Å, 0.99 Å, 1.36 Å, and 1.40 Å, respectively [49–51], indicating that Ce^{3+} and Ca^{2+} and F^- and O^{2-} exhibit almost similar ionic radii. When SA interacts with the fluorite surface, the surface Ca^{2+} ions leave approximately 4/8 of the space for the attachment of O^{2-} ions in SA. Conversely, when SA interacts with the bastnaesite surface, the surface Ce^{3+} ions leave 4/9 of the space. In addition, F^- and Ce^{3+} ions in the surface of bastnaesite are in the same plane, which negatively effects the adsorption between Ce^{3+} ions and the -COO- groups in SA. As a result, the -COO- groups in SA can coordinate with Ca^{2+} on the fluorite surface but are unable to coordinate with Ce^{3+} on the bastnaesite surface due to electrostatic repulsion and steric hindrance, as shown in Fig. 14.

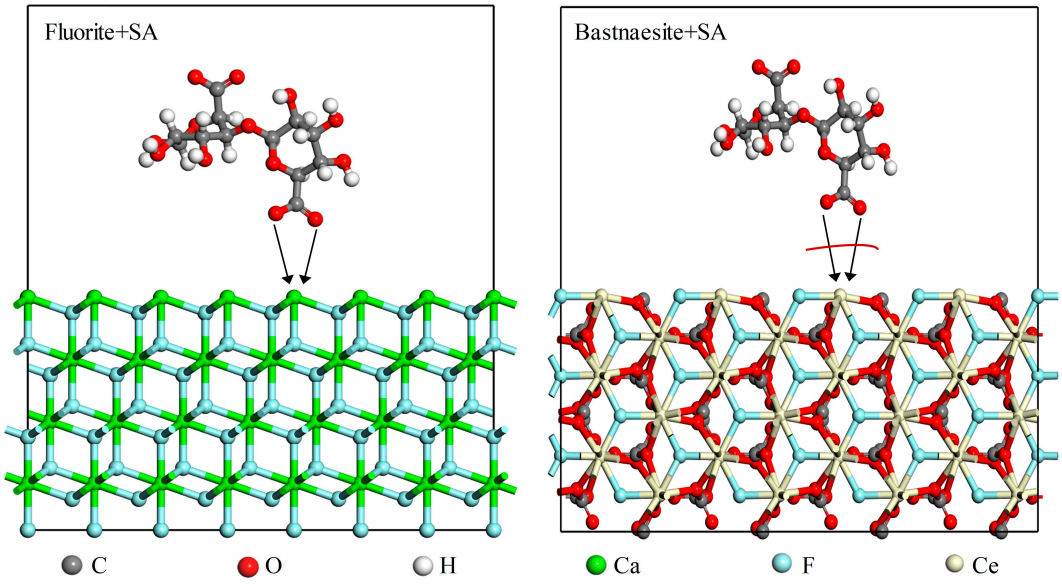

Figure 14. Schematic diagram of the adsorption model of SA on the surface of bastnaesite and fluorite.

The ability of metal ions to complex SA is another important factor affecting the selective adsorption of SA in this flotation system. Both bastnaesite and fluorite are slightly soluble in water, generating free metal ions. These metal ions are readily hydrolyzed to form metal hydroxides that reattach to the surface of the respective minerals [17]. Because of the different electronic structures, these metal ions or their metal hydroxides have different complexing abilities to SA. It has been found that the carboxylatec omplexation equilibrium constant (lg*K*) of calcium ions is much larger than that of rare earth ions [52, 53], which means that SA is more readily adsorbed on the surface of fluorite compared to bastnaesite. As a result, the hydrophilicity of SA results in the depression of fluorite, while exerting only a slight effect on bastnaesite.

4. Conclusion

In the flotation of bastnaesite and fluorite, SA, as an environmentally friendly depressant, exerted selective depressing effects. The gap in recovery reduction between fluorite and bastnaesite

was more than 65% under desirable conditions, that is, pH of about 9, SA concentration of 25 mg/L, and OHA concentration of 1.57×10^{-3} mol/L. From the results of adsorption density, zeta potential measurement, FTIR, and XPS, it can be concluded that SA is chemically anchored to the fluorite surface and impedes the subsequent adsorption of OHA as a collector and that SA interacts weakly with bastnaesite, exerting no effect on the adsorption of OHA.

CRediT authorship contribution statement: Chunlei, Guo: Methodology, Writing - original draft. Shaochun, Hou: Visualization. Weiwei, Wang: Methodology, Resources. Qiang Li: Software.

Declaration of Competing Interest: The authors declare that they have no known competing financial interests or personal relationships that might influence the work presented in this paper.

Acknowledgments: The authors sincerely acknowledge the support from the Natural Science Foundation of Inner Mongolia Autonomous Region (2023LHMS05050) and the National Key Research and Development Program of China (2022YFC2905300) projects.

References

1. Chelgani, S.C.; Rudolph, M.; Leistner, T.; Gutzmer, J.; Peuker, U.A. A Review of Rare Earth Minerals Flotation: Monazite and Xenotime. *International Journal of Mining Science and Technology* **2015**, *25*, 877–883, doi: 10.1016/j.ijmst.2015.09.002.
2. Jung, M.; Tadesse, B.; Dick, C.; Logan, A.; Dyer, L.; Albijanic, B. Influence of Monovalent and Divalent Cations on Monazite Flotation. *Colloids and Surfaces A: Physicochemical and Engineering Aspects* **2022**, *653*, 129975, doi: 10.1016/j.colsurfa.2022.129975.
3. Zhang, W.; Honaker, R.Q.; Groppo, J.G. Flotation of Monazite in the Presence of Calcite Part I: Calcium Ion Effects on the Adsorption of Hydroxamic Acid. *Minerals Engineering* **2017**, *100*, 40–48, doi: 10.1016/j.mineng.2016.09.020.
4. Cao, Z.; Cao, Y.; Qu, Q.; Zhang, J.; Mu, Y. Separation of Bastnäsite from Fluorite Using Ethylenediamine Tetraacetic Acid as Depressant. *Minerals Engineering* **2019**, *134*, 134–141, doi: 10.1016/j.mineng.2019.01.030.
5. Guo, C.; Hou, S.; Wang, W.; Jin, H. Surface Chemistry of Xanthan Gum Interactions with Bastnaesite and Fluorite during Flotation. *Minerals Engineering* **2022**, *189*, 107891, doi: 10.1016/j.mineng.2022.107891.
6. Wang, Z.; Wu, H.; Xu, Y.; Shu, K.; Yang, J.; Luo, L.; Xu, L. Effect of Dissolved Fluorite and Barite Species on the Flotation and Adsorption Behavior of Bastnaesite. *Separation and Purification Technology* **2020**, *237*, 116387, doi: 10.1016/j.seppur.2019.116387.
7. Marion, C.; Li, R.; Waters, K.E. A Review of Reagents Applied to Rare-Earth Mineral Flotation. *Advances in Colloid and Interface Science* **2020**, *279*, 102142, doi: 10.1016/j.cis.2020.102142.
8. Xu, Y.; Xu, L.; Wu, H.; Wang, Z.; Shu, K.; Fang, S.; Zhang, Z. Flotation and Co–Adsorption of Mixed Collectors Octanohydroxamic Acid/Sodium Oleate on Bastnaesite. *Journal of Alloys and Compounds* **2020**, *819*, 152948, doi: 10.1016/j.jallcom.2019.152948.
9. Zhang, X.; Du, H.; Wang, X.; Miller, J.D. Surface Chemistry Aspects of Bastnaesite Flotation with Octyl Hydroxamate. *International Journal of Mineral Processing* **2014**, *133*, 29–38, doi: 10.1016/j.minpro.2014.08.009.
10. Yang, Z. Synthesis of 3-Hydroxy-2-Naphthyl Hydroxamic Acid Collector: Flotation Performance and Adsorption Mechanism on Bastnaesite. *J. South. Afr. Inst. Min. Metall.* **2017**, *117*, 593–598, doi: 10.17159/2411-9717/2017/v117n6a10.
11. Nie, Q.; Qiu, T.; Yan, H.; Li, Y. Flotation Separation of Bastnaesite from Fluorite with an Eco-Friendly Depressant Polyepoxysuccinic Acid and Its Depression Mechanism. *Applied Surface Science* **2022**, *590*, 152941, doi: 10.1016/j.apsusc.2022.152941.
12. Pradip; Fuerstenau, D.W. The Role of Inorganic and Organic Reagents in the Flotation Separation of Rare-Earth Ores. *International Journal of Mineral Processing* **1991**, *32*, 1–22, doi: 10.1016/0301-7516(91)90016-C.
13. Leal, D.; Matsuhiro, B.; Rossi, M.; Caruso, F. FT-IR Spectra of Alginic Acid Block Fractions in Three Species of Brown Seaweeds. *Carbohydrate Research* **2008**, *343*, 308–316, doi: 10.1016/j.carres.2007.10.016.
14. Corpuz, A.G.; Pal, P.; Banat, F.; Haija, M.A. Enhanced Removal of Mixed Metal Ions from Aqueous Solutions Using Flotation by Colloidal Gas Aphrons Stabilized with Sodium Alginate. *Separation and Purification Technology* **2018**, *202*, 103–110, doi: 10.1016/j.seppur.2018.03.043.
15. Shu, K.; Xu, L.; Wu, H.; Tang, Z.; Luo, L.; Yang, J.; Xu, Y.; Feng, B. Selective Flotation Separation of Spodumene from Feldspar Using Sodium Alginate as an Organic Depressant. *Separation and Purification Technology* **2020**, *248*, 117122, doi: 10.1016/j.seppur.2020.117122.

16. Pan, G.; Zhang, G.; Shi, Q.; Chen, W. The Effect of Sodium Alginate on Chlorite and Serpentine in Chalcopyrite Flotation. *Minerals* **2019**, *9*, 196, doi: 10.3390/min9030196.
17. Chen, W.; Chen, T.; Bu, X.; Chen, F.; Ding, Y.; Zhang, C.; Deng, S.; Song, Y. The Selective Flotation of Chalcopyrite against Galena Using Alginate as a Depressant. *Minerals Engineering* **2019**, *141*, 105848, doi: 10.1016/j.mineng.2019.105848.
18. Chen, W.; Feng, Q.; Zhang, G.; Yang, Q.; Zhang, C. The Effect of Sodium Alginate on the Flotation Separation of Scheelite from Calcite and Fluorite. *Minerals Engineering* **2017**, *113*, 1–7, doi: 10.1016/j.mineng.2017.07.016.
19. Shu, K.; Xu, L.; Wu, H.; Tang, Z.; Luo, L.; Yang, J.; Xu, Y.; Feng, B. Selective Flotation Separation of Spodumene from Feldspar Using Sodium Alginate as an Organic Depressant. *Separation and Purification Technology* **2020**, *248*, 117122, doi: 10.1016/j.seppur.2020.117122.
20. Fu, Y.; Yin, W.; Yang, B.; Li, C.; Zhu, Z.; Li, D. Effect of Sodium Alginate on Reverse Flotation of Hematite and Its Mechanism. *Int J Miner Metall Mater* **2018**, *25*, 1113–1122, doi: 10.1007/s12613-018-1662-z.
21. Xu, Y.; Xu, L.; Wu, H.; Wang, Z.; Shu, K.; Fang, S.; Zhang, Z. Flotation and Co–Adsorption of Mixed Collectors Octanohydroxamic Acid/Sodium Oleate on Bastnaesite. *Journal of Alloys and Compounds* **2020**, *819*, 152948, doi: 10.1016/j.jallcom.2019.152948.
22. Guo, C.; Hou, S.; Jin, H.; Wang, W. Adsorption of Tannic Acid as Depressant in the Flotation Separation of Fluorite and Bastnaesite. *Mineral Processing and Extractive Metallurgy* **2023**, *132*, 172–184, doi: 10.1080/25726641.2023.2243198.
23. Jong, K.; Paek, I.; Kim, Y.; Li, I.; Jang, D. Flotation Mechanism of a Novel Synthesized Collector from Evodiaefructus onto Fluorite Surfaces. *Minerals Engineering* **2020**, *146*, 106017, doi: 10.1016/j.mineng.2019.106017.
24. Tian, J.; Xu, L.; Sun, W.; Zeng, X.; Fang, S.; Han, H.; Hong, K.; Hu, Y. Use of $Al_2(SO_4)_3$ and Acidified Water Glass as Mixture Depressants in Flotation Separation of Fluorite from Calcite and Celestite. *Minerals Engineering* **2019**, *137*, 160–170, doi: 10.1016/j.mineng.2019.04.011.
25. Filippova, I.V.; Filippov, L.O.; Duverger, A.; Severov, V.V. Synergetic Effect of a Mixture of Anionic and Nonionic Reagents: Ca Mineral Contrast Separation by Flotation at Neutral pH. *Minerals Engineering* **2014**, *66–68*, 135–144, doi: 10.1016/j.mineng.2014.05.009.
26. Jordens, A.; Marion, C.; Kuzmina, O.; Waters, K.E. Surface Chemistry Considerations in the Flotation of Bastnäsite. *Minerals Engineering* **2014**, *66–68*, 119–129, doi: 10.1016/j.mineng.2014.04.013.
27. Owens, C.L.; Nash, G.R.; Hadler, K.; Fitzpatrick, R.S.; Anderson, C.G.; Wall, F. Zeta Potentials of the Rare Earth Element Fluorcarbonate Minerals Focusing on Bastnäsite and Parisite. *Advances in Colloid and Interface Science* **2018**, *256*, 152–162, doi: 10.1016/j.cis.2018.04.009.
28. Yu, X.; Zhang, R.; Yang, S.; Liu, C.; He, G.; Wang, H.; Wang, J. A Novel Decanedioic Hydroxamic Acid Collector for the Flotation Separation of Bastnäsite from Calcite. *Minerals Engineering* **2020**, *151*, 106306, doi: 10.1016/j.mineng.2020.106306.
29. Meng, Q.; Feng, Q.; Shi, Q.; Ou, L. Studies on Interaction Mechanism of Fine Wolframite with Octyl Hydroxamic Acid. *Minerals Engineering* **2015**, *79*, 133–138, doi: 10.1016/j.mineng.2015.05.015.
30. Ni, X.; Liu, Q. The Adsorption and Configuration of Octyl Hydroxamic Acid on Pyrochlore and Calcite. *Colloids and Surfaces A: Physicochemical and Engineering Aspects* **2012**, *411*, 80–86, doi: 10.1016/j.colsurfa.2012.07.005.
31. Xu, H.; Zhong, H.; Tang, Q.; Wang, S.; Zhao, G.; Liu, G. A Novel Collector 2-Ethyl-2-Hexenoic Hydroxamic Acid: Flotation Performance and Adsorption Mechanism to Ilmenite. *Applied Surface Science* **2015**, *353*, 882–889, doi: 10.1016/j.apsusc.2015.06.072.
32. Zhong, C.; Feng, B.; Zhang, W.; Zhang, L.; Guo, Y.; Wang, T.; Wang, H. The Role of Sodium Alginate in the Flotation Separation of Apatite and Dolomite. *Powder Technology* **2020**, *373*, 620–626, doi: 10.1016/j.powtec.2020.07.007.
33. Xiong, W.; Deng, J.; Zhao, K.; Wang, W.; Wang, Y.; Wei, D. Bastnaesite, Barite, and Calcite Flotation Behaviors with Salicylhydroxamic Acid as the Collector. *Minerals* **2020**, *10*, 282, doi: 10.3390/min10030282.
34. Zhong, C.; Feng, B.; Zhang, W.; Zhang, L.; Guo, Y.; Wang, T.; Wang, H. The Role of Sodium Alginate in the Flotation Separation of Apatite and Dolomite. *Powder Technology* **2020**, *373*, 620–626, doi: 10.1016/j.powtec.2020.07.007.
35. Huang, L.; Zeng, Q.; Hu, L.; Hu, Y.; Zhong, H.; He, Z. The Contribution of Long-Terms Static Interactions between Minerals and Flotation Reagents for the Separation of Fluorite and Calcite. *Minerals* **2019**, *9*, 699, doi: 10.3390/min9110699.
36. Patra, A.; Taner, H.A.; Bordes, R.; Holmberg, K.; Larsson, A.-C. Selective Flotation of Calcium Minerals Using Double-Headed Collectors. *Journal of Dispersion Science and Technology* **2019**, *40*, 1205–1216, doi: 10.1080/01932691.2018.1503547.

37. Zhu, X.; Lyu, X.; Wang, Q.; Qiu, J.; Wang, S.; Liu, X.; Li, L. Clean Utilization of Waste Oil: Soap Collectors Prepared by Alkaline Hydrolysis for Fluorite Flotation. *Journal of Cleaner Production* **2019**, *240*, 118179, doi: 10.1016/j.jclepro.2019.118179.
38. Cao, S.; Cao, Y.; Liao, Y.; Ma, Z. Depression Mechanism of Strontium Ions in Bastnaesite Flotation with Salicylhydroxamic Acid as Collector. *Minerals* **2018**, *8*, 66, doi: 10.3390/min8020066.
39. Lin, Y.; Chen, C.; Wang, W.; Jiang, Y.; Cao, X. Beneficial Effects and Mechanism of Lead Ions for Bastnaesite Flotation with Octyl Hydroxamic Acid Collector. *Minerals Engineering* **2020**, *148*, 106199, doi: 10.1016/j.mineng.2020.106199.
40. Bêche, E.; Charvin, P.; Perarnau, D.; Abanades, S.; Flamant, G. Ce 3d XPS Investigation of Cerium Oxides and Mixed Cerium Oxide ($Ce_xTi_yO_z$). *Surface & Interface Analysis* **2008**, *40*, 264–267, doi: 10.1002/sia.2686.
41. Perry, D.L.; Tsao, L.; Brittain, H.G. X-Ray Photoelectron and Infrared Spectroscopic Studies of the Decarboxylation/Oxidation of Cerium (III) Carbonate Octahydrate. *J Mater Sci Lett* **1984**, *3*, 1017–1019, doi: 10.1007/BF00720345.
42. Zhang, C.; Hu, Y.; Sun, W.; Zhai, J.; Yin, Z.; Guan, Q. Effect of Phytic Acid on the Surface Properties of Scheelite and Fluorite for Their Selective Flotation. *Colloids and Surfaces A: Physicochemical and Engineering Aspects* **2019**, *573*, 80–87, doi: 10.1016/j.colsurfa.2019.04.044.
43. Cui, Y.; Jiao, F.; Wei, Q.; Wang, X.; Dong, L. Flotation Separation of Fluorite from Calcite Using Sulfonated Lignite as Depressant. *Separation and Purification Technology* **2020**, *242*, 116698, doi: 10.1016/j.seppur.2020.116698.
44. Zhang, Z.; Cao, Y.; Ma, Z.; Liao, Y. Impact of Calcium and Gypsum on Separation of Scheelite from Fluorite Using Sodium Silicate as Depressant. *Separation and Purification Technology* **2019**, *215*, 249–258, doi: 10.1016/j.seppur.2019.01.021.
45. Hecht, H.; Srebnik, S. Structural Characterization of Sodium Alginate and Calcium Alginate. *Biomacromolecules* **2016**, *17*, 2160–2167, doi: 10.1021/acs.biomac.6b00378.
46. Cao, S.; Cao, Y.; Ma, Z.; Liao, Y.; Zhang, X. Structural and Electronic Properties of Bastnaesite and Implications for Surface Reactions in Flotation. *Journal of Rare Earths* **2020**, *38*, 332–338, doi: 10.1016/j.jre.2019.04.020.
47. Gao, Z.; Wang, C.; Sun, W.; Gao, Y.; Kowalczuk, P.B. Froth Flotation of Fluorite: A Review. *Advances in Colloid and Interface Science* **2021**, *290*, 102382, doi: 10.1016/j.cis.2021.102382.
48. Tasker, P.W. The Structure and Properties of Fluorite Crystal Surfaces. *J. Phys. Colloques* **1980**, *41*, C6-488-C6-491, doi: 10.1051/jphyscol: 19806127.
49. Jia, Y.Q. Crystal Radii and Effective Ionic Radii of the Rare Earth Ions. *Journal of Solid State Chemistry* **1991**, *95*, 184–187, doi: 10.1016/0022-4596(91)90388-X.
50. Pauling, L. The Sizes of Ions and the Structure of Ionic Crystals. *J. Am. Chem. Soc.* **1927**, *49*, 765–790, doi: 10.1021/ja01402a019.
51. Shannon, R.D.; Prewitt, C.T. Effective Ionic Radii in Oxides and Fluorides. *Acta Crystallogr B Struct Sci* **1969**, *25*, 925–946, doi: 10.1107/S0567740869003220.
52. Janicki, R.; Mondry, A.; Starynowicz, P. Carboxylates of Rare Earth Elements. *Coordination Chemistry Reviews* **2017**, *340*, 98–133, doi: 10.1016/j.ccr.2016.12.001.
53. Sun, W.; Han, H.; Sun, W.; Wang, R. Novel Insights into the Mechanism of Lime Method Based on Calcium Dioleate and Mineral Surface Transformation. *J. Cent. South Univ.* **2023**, *30*, 2983–2992, doi: 10.1007/s11771-023-5421-6.